RSC Advances

PAPER

View Article Online
View Journal | View Issue

Cite this: *RSC Adv.*, 2021, **11**, 29416

Controllable growth of Cu–Bi co-doped ZnO nanospheres on cotton fabrics and a study on their photocatalytic performance in visible light

Liuqi Cao, Liming Wang,* Lihui Xu,* Yong Shen, Mingrui Xie and Huimin Hao

Cu–Bi co-doped ZnO nanospheres were obtained by adopting Bi and Cu to dope ZnO to improve their photocatalytic performance in the visible region. Cu–Bi co-doped ZnO nanospheres were successfully grown on the surface of cotton fabric by a sol–gel assisted hydrothermal method with citric acid as a morphology control agent. The obtained products were characterized by X-ray diffraction analysis (XRD), scanning electron microscopy (SEM), X-ray photoelectron spectroscopy (XPS) and diffuse reflectance spectroscopy (DRS). The results showed that the size of ZnO nanospheres was about 200 nm and doping with Cu and Bi did not change their morphology. Cu–Bi co-doped ZnO nanospheres presented a hexagonal wurtzite structure with high crystallinity; meanwhile, their band gap was also obviously reduced due to doping, from 3.24 eV to 2.82 eV. Cu–Bi co-doped ZnO nanospheres endowed the cotton fabric with excellent UV (ultraviolet) resistance with a UPF (Ultraviolet Protection Factor) value of 283.54 after 40 washes. Cotton fabric with 3% Bi–5% Cu co-doped ZnO on the surface showed 98.66% degradation of methylene blue (MB) solution under visible light irradiation for 150 min, indicating remarkable photocatalytic performance.

Received 10th July 2021
Accepted 17th August 2021

DOI: 10.1039/d1ra05317e

rsc.li/rsc-advances

1. Introduction

In recent years, multifunctional textiles, including UV resistance, photocatalytic, antimicrobial, and flame retardant properties, have been studied continuously and have attracted plenty of attention due to their potential applications in industrial production.[1–6] Cotton fabric has been one of the most used fabrics in the market because of its excellent hygroscopic property, thermal insulation and wearing comfort.[7,8] However, in daily life, cotton fabric is not able to provide effective UV resistance and photocatalytic performance, which largely limits its practical application.[9,10]

ZnO as a wide band gap (3.37 eV) semiconductor material has great chemical stability and biocompatibility, and has high exciton binding energy (60 meV) at room temperature; most research studies chose to attach or grow nanomaterials on the fabric to endow or change the performance of the fabric.[11–14] For example, Irmak *et al.*[15] reported the growth of ZnO nanowires in carbon fibres and proved that ZnO nanowires significantly improved the photocatalytic performance of carbon fibres. Sha *et al.*[16] successfully prepared single-crystalline wurtzite ZnO nanorods on carbon fibers and experimental results showed an outstanding degradation of MB solution and good recyclability. Most prepared ZnO had mainly one-dimensional and two-dimensional morphologies in the current literature, and the multidimensional morphology of ZnO was seldom reported;[17–19] moreover, ZnO only reacts in the ultraviolet region due to its nature, so researchers adopted doping modification to expand its application in visible light.[20–22] Nithya *et al.*[23] introduced Mn doped nano-sized ZnO, which was prepared by a chemical precipitation method, and the results showed that the band gap of Mn doped ZnO was obviously reduced, and the degradation of BG dye solution reached 97.47% under solar light, which showed outstanding photocatalytic performance. Wang *et al.*[24] reported the flower-like ZnO doped with Ce and the results showed that the photocatalytic effect under solar irradiation was 80.56% higher than that of pure ZnO. However, at present, most reports mainly focus on single-element doping, while less research emphasis has been placed on multi-element co-doping; the photocatalytic activity of ZnO under visible light is not improved to the greater extent.[25–27]

According to literature research, it is very difficult to grow ZnO nanospheres with a controllable morphology on cotton fabric with a soft substrate, because many factors in the reaction process will affect the morphology. Meanwhile, doping with elements has always been the focus of improving the photocatalytic performance of ZnO. In this paper, using the sol–gel method and hydrothermal method, by controlling the citric acid, reaction temperature and time, the growth process of ZnO nanospheres was studied along with reaction element influence on morphology, and at the same time Bi and Cu were mixed together, which greatly expanded the nano ZnO light response range, and improved the visible light photocatalytic

School of Textiles and Fashion, Shanghai University of Engineering Science, Shanghai 201620, China. E-mail: nirvanaclq@163.com; Tel: +86-17856927352

performance of the samples. The prepared samples were characterized by X-ray diffraction (XRD), scanning electron microscopy (SEM), X-ray photoelectron spectroscopy (XPS) and diffuse reflectance spectroscopy (DRS); the results showed excellent UV resistance and excellent photocatalytic performance of Bi–Cu co-doping in visible light.

2. Experiment

2.1 Materials

The used cotton fabrics were purchased from Shanghai Songzhi Textile Fabric Co., Ltd. Acetone, ethyl alcohol (C_2H_6O), magnesium chloride hexahydrate ($MgCl_2 \cdot 6H_2O$), zinc acetate dihydrate ($C_4H_6O_4Zn \cdot 2H_2O$), zinc nitrate hexahydrate ($Zn(NO_3)_2 \cdot 6H_2O$), sodium hydroxide (NaOH), hexamethylene tetramine ($C_6H_{12}N_4$), citric acid ($C_6H_8O_7 \cdot H_2O$), bismuth(III) nitrate pentahydrate ($Bi(NO_3)_3 \cdot 5H_2O$) and copper(II) nitrate trihydrate ($Cu(NO_3)_2 \cdot 3H_2O$) were purchased from Sinopharm Chemical Reagent Co., Ltd. 3-(Trimethoxysilyl)propyl methacrylate (KH-570) was purchased from Sigma-Aldrich. All the chemicals were of analytic grade and used without further purification.

2.2 Preparation of a ZnO crystal seed layer on cotton fabric (ZnO crystal seed@cotton fabric)

A ZnO crystal seed layer was coated on cotton fabric *via* the sol–gel method. Firstly, the pure cotton fabrics were washed with distilled water and ethyl alcohol three times respectively, and dried at 85 °C for 30 min. Then, the treated cotton fabric (5 cm × 5 cm) was placed into a mixed solution, which was prepared by dissolving 0.52 g $MgCl_2 \cdot 6H_2O$ and 2% KH-570 in 250 mL of distilled water, and stirred for 1 h at 80 °C, and finally, the KH-570 cross-linked cotton fabric was obtained at 85 °C for 30 min.

ZnO seed solution was prepared by respectively dissolving 1.35 g $C_4H_6O_4Zn \cdot 2H_2O$ and 0.75 g NaOH in 65 mL of C_2H_6O. Then, the 65 mL $C_4H_6O_4Zn \cdot 2H_2O/C_2H_6O$ and $NaOH/C_2H_6O$ were fused in a three-necked flask at 60 °C for 2 h. KH-570 cross-linked cotton fabric was ultrasonically soaked in ZnO seed solution for 30 min, followed by three dipping and three rolling by a padder, and dried at 80 °C.

2.3 ZnO nanospheres grown on cotton fabric (ZnO@cotton fabric)

ZnO nanospheres were grown on the cotton fabric surface using a hydrothermal method with growth solution. A 50 mL growth solution was made by mixing 0.04 mol L^{-1} $Zn(NO_3)_2 \cdot 6H_2O$ and 0.02 mol L^{-1} $C_6H_{12}N_4$, and a certain amount of 0.5 M water solution of trisodium citrate dihydrate was added as a morphology control agent. The cotton fabric covered with crystal seeds was placed in a constant temperature shock water bath for hydrothermal reaction at 60 °C, 75 °C, and 90 °C for 3, 4, and 5 hours. Subsequently, the cotton fabric was taken out and dried at 80 °C.

2.4 Bi/Cu doped ZnO nanospheres grown on cotton fabric (Bi/Cu doped ZnO@cotton fabric)

Referring to the preparation method of growth solution, Bi (1%, 2%, 3%, and 4%) and Cu (1%, 3%, and 5%) were added into the above solution, and then put in a conical flask under ultrasonic wave to dissolve or disperse them. Meanwhile, adopted the same hydrothermal reaction method at 70 °C for 4 hours, and dried at 80 °C.

2.5 Characterization

The crystal structures of the ZnO@cotton fabric and Bi/Cu doped ZnO@cotton fabric were determined using powder X-ray diffraction (XRD, Bruker D8 Advance, Germany) at a scan rate of 1° min^{-1}, using Cu Kα radiation (40 kV, 35 mA, k = 0.1789 nm). A scanning electron microscope (SEM, Hitachi S4800, Japan) was used to observe the microstructure of ZnO nanospheres coated with cotton fabric. The chemical state of the elements on the cotton surface was tested by X-ray photoelectron spectroscopy (XPS, Thermo Scientific K-Alpha, USA), with Al Kα radiation as the source (12 kV, 6 mA, vacuum >5.0×10^{-7} mBar). Optical properties of the cotton fabric coated with ZnO nanospheres were studied in the UV-vis region using Diffuse Reflectance Spectroscopy (DRS, Shimadzu UV-3600, Japan) between 200 and 800 nm. Bandgap energy (E_g) was calculated by Tauc relation, according to the Kubelka–Munk theory.

2.6 UV resistance

The UV resistance capability of ZnO@cotton fabric and Bi/Cu doped ZnO@cotton fabric was evaluated by measuring the percentage transmission of UV radiations on an ultraviolet transmittance analyzer (UV-2000, USA) on the basis of AATCC 183-2000 standard. Ultraviolet Protection Factor (UPF) was calculated by the average of three measurements. Eqn (1) was used to calculate the UPF.

$$\mathrm{UPF} = \frac{\sum_{280\ \mathrm{nm}}^{400\ \mathrm{nm}} E_\lambda S_\lambda E \Delta_\lambda}{\sum_{280\ \mathrm{nm}}^{400\ \mathrm{nm}} E \lambda S_\lambda T_\lambda \Delta_\lambda} \quad (1)$$

where S_λ is the solar spectral irradiance, E_λ is the relative erythemal spectral response, T_λ is the average spectral transmittance of the sample and Δ_λ is the measured wavelength interval in nanometers.

2.7 Photocatalysis

The photocatalysis properties of ZnO@cotton fabric and Bi/Cu doped ZnO@cotton fabric were tested *via* degradation efficiency for methylene blue solution (MB). The cotton fabric was cut into 0.5 cm × 0.5 cm, and after that, placed in a quartz tube containing 100 mL 15 mg L^{-1} methylene blue dye and dark reacted for 1 hour in photochemical reaction apparatus (BILON-GHX-V China). After the dark reaction, a visible light or UV lamp was turned on for photocatalytic reaction; a 100 W halogen lamp was used as the visible light source, while the ultraviolet lamp had an intensity of 80 W. During the whole reaction

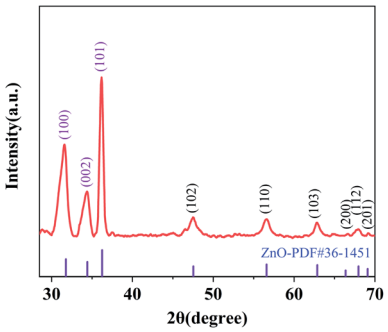

Fig. 1 XRD pattern of ZnO nanospheres on the cotton fabric surface.

process, MB solution was absorbed and centrifuged (6000 rpm, 5 min) every 30 min, and then the supernatant after centrifugation was taken to a UV-vis spectrometer (UV-2600, Japan) for analysis of the photocatalytic degradation rate. Degradation efficiency (η) is calculated by formula (2):

$$\eta = \frac{C_0}{C} \times 100\% = \frac{A_0}{A} \times 100\% \quad (2)$$

where C_0 is the initial dye concentration, C is the instant dye concentration, A_0 is the initial absorbance and A is the instant absorbance.

3. Results and discussion

3.1 X-ray diffraction (XRD)

The XRD pattern was analysed to confirm the existence of ZnO grown on cotton fabric. As shown in Fig. 1, the crystal structure of ZnO belongs to hexagonal wurtzite and the peaks at 31.58°, 34.36°, 36.18°, 47.48°, 56.54°, 62.82°, 66.62°, 67.92° and 69.2° corresponded to (100), (002), (101), (102), (110), (103), (200), (112) and (201) crystal lattice planes, respectively. All peaks of ZnO were in keeping with the standard card no. 36-1451 of the International Center for Diffraction Data (ICDD) database, and no other peaks were observed in the XRD spectrum.[28,29] The grain size of ZnO was calculated by the Debye–Scherrer formula and the mean grain size was about 346.32 nm; therefore, the results of XRD patterns show that nano-sized ZnO certainly exists on the surface of cotton fabric and there are no other impurities.

Fig. 2 shows the XRD spectrum of ZnO doped with different ratios of bismuth (1%, 2%, 3%, and 4%) and copper (1%, 3%, and 5%). The crystal structure of ZnO hexagonal wurtzite showed no change under the doping with Bi and Cu, which could be seen form the XRD pattern. When doped with low concentrations of Bi (1%, 2%, and 3%), the diffraction peak moved in the lower angle direction (Fig. 2(a)), which was attributed to the larger Bi ions in the crystal replacing the Zn ions, causing the lattice to expand. This trend changed at 4% of Bi concentration, because of the generation of other impurities due to excessive Bi.[30] As for Cu doped ZnO shown in Fig. 2(b), the ionic radius of Cu^{2+} is close to that of Zn^{2+}, and it has compatibility; therefore, with the increase of Cu doping concentration, the diffraction peaks generally shifted to a high angle. With the Cu doping concentration reaching 8%, the diffraction peak of CuO appears in the XRD pattern, indicating that when the doping concentration exceeds 5%, the CuO in the system is gradually generated and the impurity phase is formed,

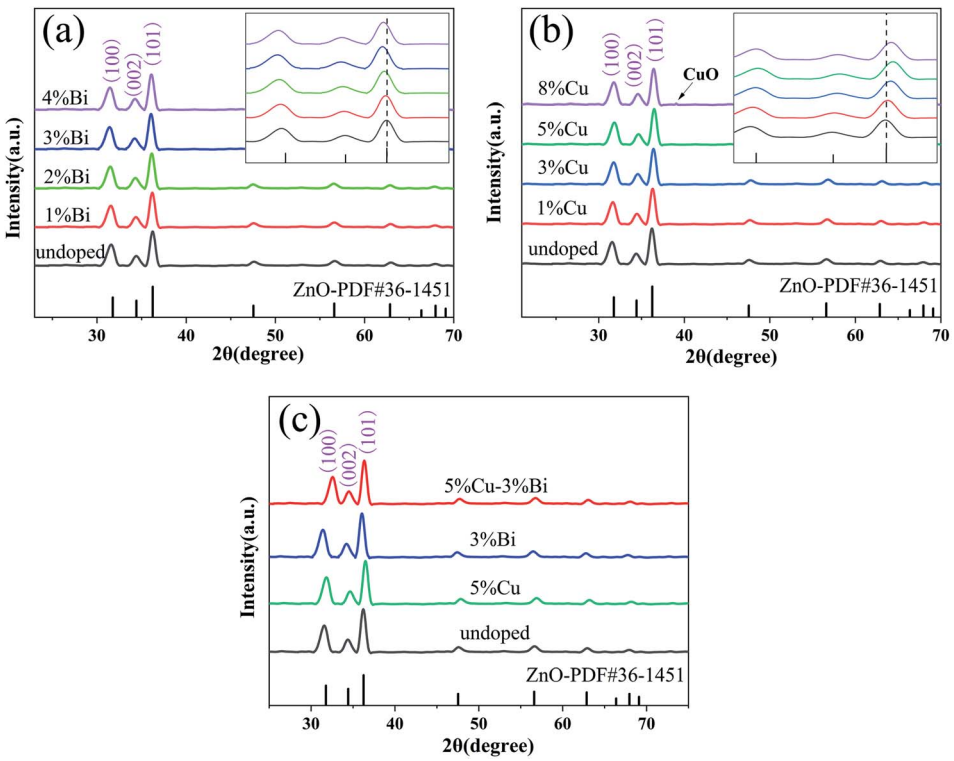

Fig. 2 XRD patterns of Bi (a), Cu (b), and Bi–Cu (c) doped ZnO nanospheres in different proportions on the cotton fabric surface.

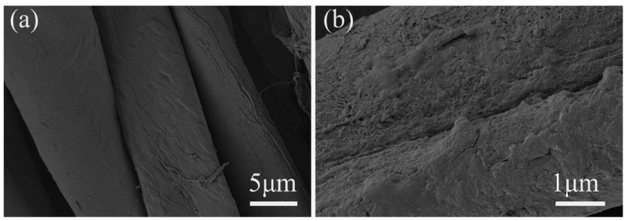

Fig. 3 SEM images of (a) pure cotton fabric and (b) ZnO crystal seed@cotton fabric.

which are consistent with that described in the literature.[31,32] Using 3% Bi and 5% Cu co-doped ZnO grown on cotton fabric showed more prominent and sharp diffraction peaks compared to single element doping, which are observed in Fig. 2(c).

3.2 Scanning electron microscope (SEM)

In order to study the growth of nano ZnO on cotton fabric and the effects of citric acid, hydrothermal reaction temperature and time on morphology growth, the growth process of spherical nano ZnO under different conditions was tested using a scanning electron microscope (SEM). Fig. 3(a and b) shows the SEM of pure cotton fabric and ZnO crystal seed@cotton fabric; as can be seen, on the surface of pure cotton fabric without other impurities, the fibre surface was smooth; by contrast, the surface of cotton fabric treated with ZnO seed solution was attached with an obvious ZnO seed layer, which provided more reaction sites and favourable conditions.

Fig. 4 shows the growth of nano ZnO on the cotton fabric surface under different reaction conditions, which illustrated the effects of citric acid solution, hydrothermal reaction temperature and time on the morphology. Fig. 4(a and b) shown the microstructure of the prepared ZnO grown without citric acid solution. It can be found that the irregular morphology of size from 1–2 μm was formed due to the character of priority grows along the *C* axis belong to ZnO and agglomeration of the ZnO nanosheets. Compared with not adding citric acid solution, the effect of growth with it as a morphology control agent is shown in Fig. 4(c); it can be evidently observed that a large amount of ZnO exists in the shape of sphere, with the size ranging from 100 nm to 200 nm, which is grown on the surface of cotton fibres evenly. The formation of spherical nano ZnO

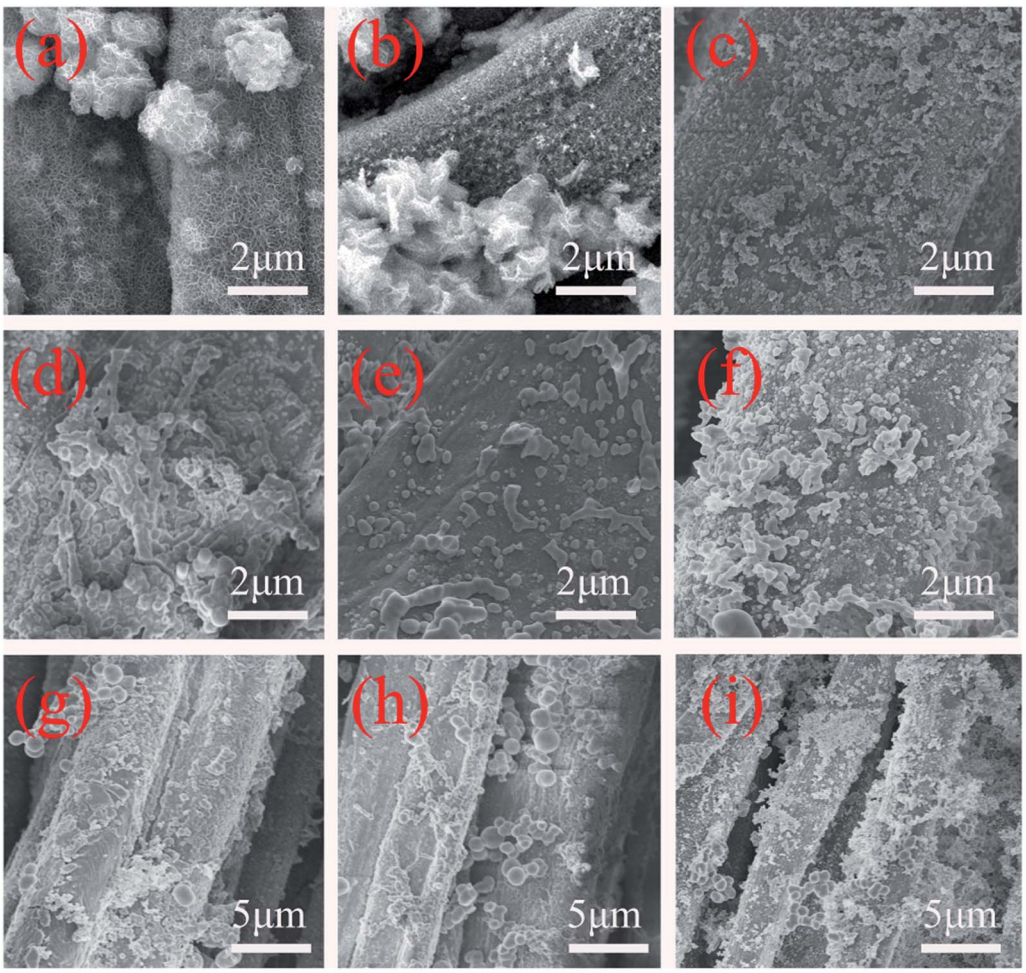

Fig. 4 SEM images of nano ZnO on the cotton fabric surface under different reaction conditions: (a–c) with and without citric acid aqueous solution added; (d–f) hydrothermal reaction temperatures at 60 °C, 75 °C, and 90 °C; (g–i) hydrothermal reaction time at 2, 4, and 6 h.

was mainly related to the pressure in the system. In a closed reaction vessel, the citric acid gradually hydrolysed and released CO_2, which increased the pressure in the system.

According to the aggregation growth theory, when multiple nanoparticles collide effectively in the reaction system, they fuse to form larger particles.

As shown in Fig. 5, in the growth process of nanoparticles, when the effective collision rate is greater than the growth rate between particles, the aggregated nanoparticles will continue to collide with other nanoparticles, and finally form the rod or line morphology; on the other hand, when the system pressure increases, the growth rate is greater than the collision rate, has gathered the particles in front of the collisions with other particles had formed a separate nanoparticle, eventually forming a spherical morphology, *etc.*[33,34] The temperature and time of hydrothermal reaction also have great influence on the morphology, as shown in Fig. 4(d–f); when the hydrothermal reaction temperature was 60 °C, the ZnO on the surface of cotton fabric was mainly spherical and rod with a size from 150 nm to 500 nm, which was mainly attributed to the low temperature and incomplete decomposition of citric acid, resulting in insufficient pressure in the system. With the temperature rising to 75 °C, the citric acid fully decomposed and released carbon dioxide, so that the growth rate in the system was greater than the effective collision rate, and the final morphology was mainly spherical and quasi-spherical. When the temperature reaches 90 °C, ZnO showed a serious agglomeration phenomenon, which may be caused by the intense reaction in the system at too high temperature, resulting in too high particle movement and collision.

The influence of hydrothermal reaction time on the morphology of ZnO was mainly reflected in the decomposition of $C_6H_{12}N_4$ in the system. When the reaction time was 2 h, $C_6H_{12}N_4$ was not completely decomposed into ammonium hydroxide to provide OH^-, resulting in a small content of nano ZnO on the surface of cotton fabric, as shown in Fig. 4(g). With the extension of the reaction time to 4 h, $C_6H_{12}N_4$ fully hydrolyzed to provide OH^-, and spherical nano ZnO was generated on the surface of cotton fabric, with a size of 150 nm to 300 nm. However, when the reaction time was prolonged to 7 h, the nano ZnO formed in the system aggregated together to form aggregates.

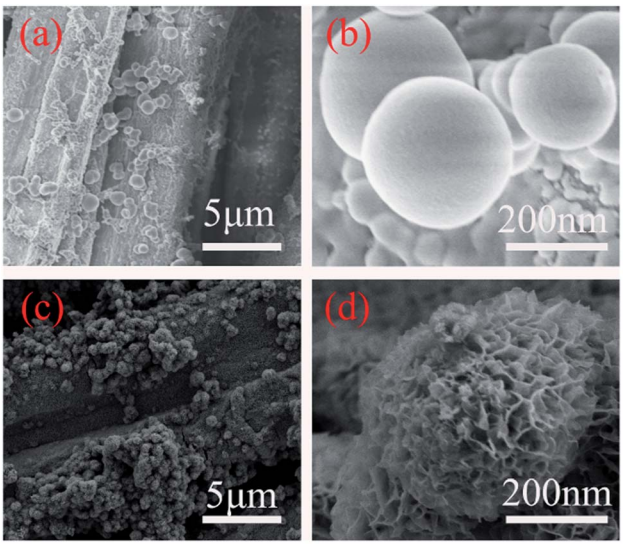

Fig. 6 SEM images of (a and b) ZnO nanospheres and (c and d) 3% Bi–5% Cu co-doped ZnO.

Fig. 6 shows the SEM images of ZnO nanospheres@cotton fabric (a and b) and Bi–Cu co-doped ZnO nanospheres@cotton fabric (c and d) with the hydrothermal reaction temperature at 60 °C, the reaction time was 4 hours, and the citric acid solution was added, which were obtained as the optimal conditions on the basis of the above experiment. As can be seen from Fig. 6(a and b), under the optimal conditions, the nano ZnO on the surface of cotton fabric was mainly spherical, with a size of 150–300 nm, and the distribution was uniform without obvious agglomeration. Fig. 6(c and d) reveals the morphology of 3% Bi–5% Cu co-doped ZnO adhering to cotton fabric. ZnO nanospheres were formed by the aggregation of nanosheets, the thickness of which was 35 nm. In fact, the surface of undoped ZnO nanospheres has a tiny porous structure which is not suitable for observation. However, the co-doped ZnO nanospheres have an obvious porous structure, which was mainly

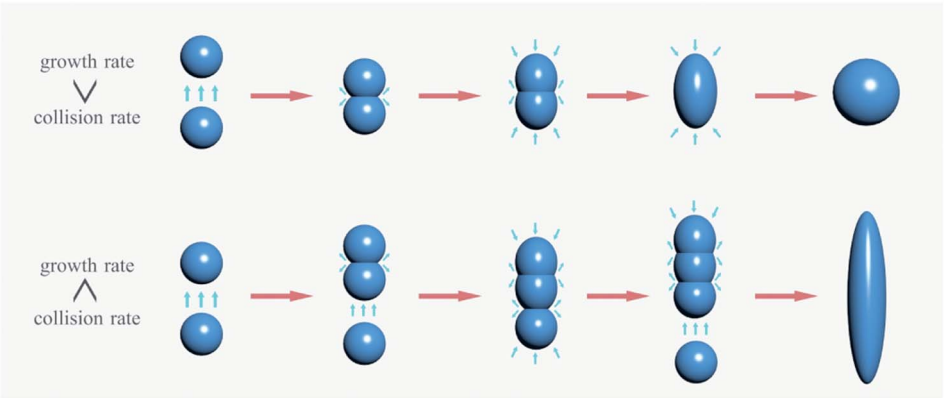

Fig. 5 Schematic diagram of aggregation growth theory.

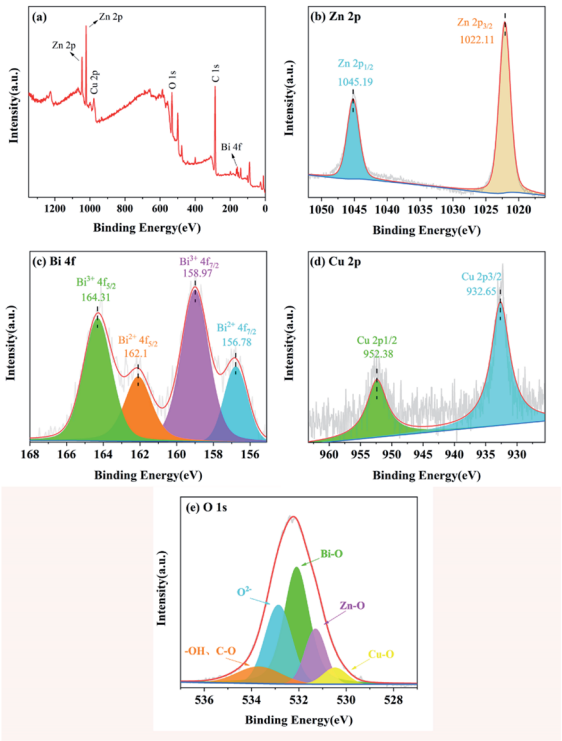

Fig. 7 XPS spectra of 3% Bi–5% Cu co-doped ZnO nanospheres on the cotton fabric surface: (a) survey scan, and (b–e) high resolution scans Zn 2p, Bi 4f, Cu 2p and O 1s respectively.

attributed to the Bi and Cu doping changing the cell factor of ZnO nanospheres; however, the overall morphology did not change. The results of SEM proved the controllable growth of ZnO nanospheres and effectiveness of citric acid solution during the process of growth.

3.3 X-ray photoelectron spectroscopy (XPS)

The surface compositions and chemical states of Bi/Cu doped ZnO@cotton fabric were determined using XPS spectra, as shown in Fig. 7. The result of scan in Fig. 7(a) shows that Zn, Bi, Cu, O and C coexisted on the surface of cotton fabric. All binding energies were corrected for the charge shift and referenced using the C 1s peak of graphitic carbon (284.3 eV). The high-resolution scan XPS of Bi 4f is shown in Fig. 7(c), the two main peaks located at 164.31 eV and 158.97 eV correspond to the Bi $4f_{5/2}$ and Bi $4f_{7/2}$ binding energies of Bi^{3+}; meanwhile, two lower peaks located at 162.1 eV and 156.78 eV were related to Bi $4f_{5/2}$ and Bi $4f_{7/2}$ binding energies of Bi^{2+}, and it was verified that Bi^{3+} was the main chemical statues in the mixture according to the XPS spectrum.[35] As for the high-resolution Zn 2p spectrum, the peaks located at 1045.19 eV and 1022.11 eV were assigned to Zn $2p_{1/2}$ and Zn $2p_{3/2}$, and the difference of binding energy between the peaks was 23.08 eV, which conforms to the standard reference of ZnO.[36]

The XPS spectrum of Cu shows two peaks located at 952.38 eV and 932.65 eV which could be ascribed to Cu $2p_{1/2}$ and Cu $2p_{3/2}$ respectively.[37] The O 1s XPS spectrum is shown in Fig. 7(e). The main peak of O 1s divides into five different peaks located at 530.54 eV, 531.34 eV, 532.18 eV, 532.98 eV, and 533.76 eV which represented five different kinds of O species in the compound. The peak at 531.34 eV was attributed to the O atom in the ZnO lattice, while the peaks at 532.18 eV and 530.54 eV are related to Bi–O and Cu–O respectively. The peak at 532.98 eV was associated with O^{2-} ions that were in oxygen-deficient regions, and the peak at 533.76 eV corresponded to surface adsorbed –OH and C–O. The result of XPS analysis certified that Bi–Cu were successfully co-doped in ZnO grown on cotton fabric.[38,39]

3.4 Ultraviolet (UV) resistance

As we know, prolonged exposure to ultraviolet light is detrimental to subcutaneous tissue, and hence the UV resistance test was performed for samples including pure, un-doped and Bi/Cu doped cotton fabric following the AATCC standard for UV resistance of textiles. The result is shown in Fig. 8(a); the Ultraviolet Protection Factor (UPF) value of pure cotton fabric was only 6.57 and ultraviolet A (UVA (310–370 nm)) and ultraviolet B (UVB (250–310 nm)) were 30.84% and 25.83% respectively, which is regarded as no ability of UV resistance. However, the sample of ZnO/cotton showed extremely low UV transmittance and prominent UV absorption ranging from 290 nm to 360 nm, and UPF reached 81.2, which proved that ZnO nanospheres were successfully grown on the surface of cotton fabric

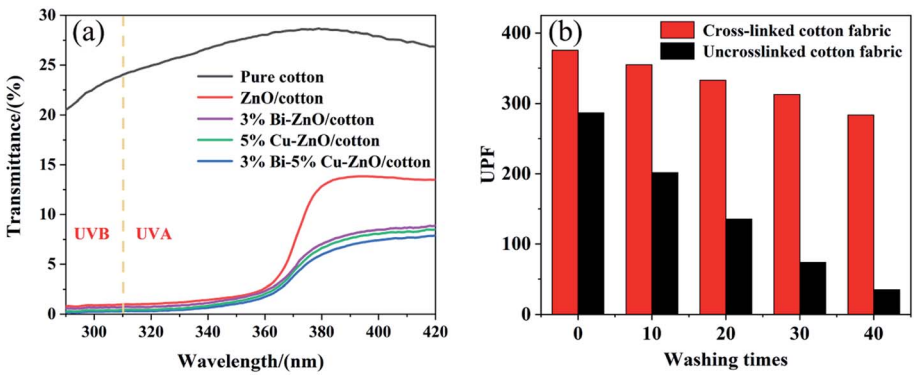

Fig. 8 Ultraviolet transmittance diagram of different samples (a) and UPF value histogram of different times (b).

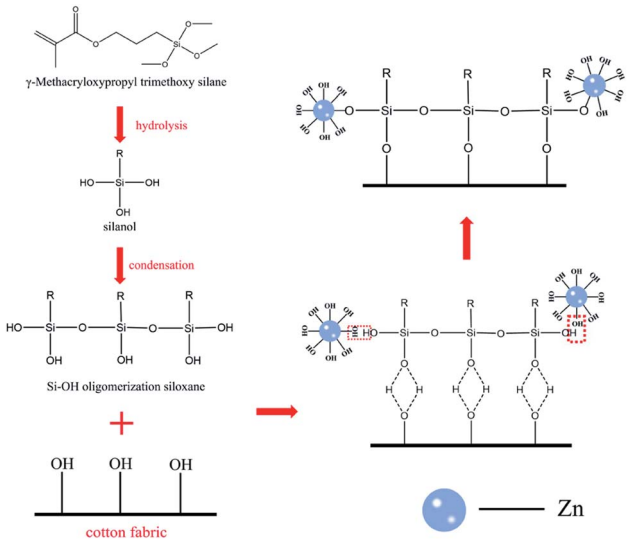

Fig. 9 Mechanism diagram of promoting the binding of ZnO to cotton fabric by KH-570.

and endowed excellent UV resistance; however, the transmittance in the UVA region was 6.23% and not up to the 50+ standard because the spectral range of ZnO was mainly in the ultraviolet region. Doping with 3% Bi–5% Cu decreased the transmittance value of UVA and UVB regions to 2.56% and 0.09% respectively, and UPF reached 375.42, which is because ZnO was an N-type semiconductor and the doping with Bi and Cu reduces the band gap and electrons in the valence band were more likely to undergo electron transitions.

Fig. 8(b) shows the change of UPF value after different washing times between the cotton crosslinking with KH-570 and untreated cotton fabric; apparently, the UV resistance performance of ZnO grown on the surface of cotton fabric without crosslinking treatment was significantly reduced after washing; the UPF value was only 43 after 40 washes. By contrast, cotton fabric with crosslinking treatment still possessed UV resistance under the same conditions. As a kind of inorganic nanomaterial, ZnO shows strong polarity, hydrophilic and oleophobic properties, and cannot combine with the hydroxyl group on the surface of cotton fabric to produce a firm binding force. The molecular structure of the silane coupling agent contains both organic groups and inorganic structures. The alkoxy group in the silane coupling agent KH-570 molecule can hydrolysate and form strong chemical bonds with inorganic materials. At the same time, chemical reactions or physical entanglement occur with organic materials to improve the compatibility between inorganic materials and organic materials.[40] In this work, silane coupling agent KH-570 is used as a bridge to improve the bonding fastness of ZnO and cotton fabric after crosslinking treatment, and the principle of KH-570 is shown in Fig. 9.

3.5 Diffuse reflectance spectrum (DRS)

Fig. 10(a) shows the absorption spectra of ZnO/cotton, 3% Bi–ZnO/cotton, 5% Cu–ZnO/cotton and 3% Bi–5% Cu co-doped ZnO/cotton, which were obtained from UV-vis diffuse reflectance data by the Kubelka–Munk formula. All samples exhibited an obvious absorption edge at 395 nm, which was mainly attributable to the existence of the energy band structure of ZnO. Compared to ZnO/cotton the absorption edges of 3% Bi-doped ZnO/cotton, 5% Cu-doped ZnO/cotton and 3% Bi–5% Cu co-doped ZnO/cotton all showed enormous absorption intensity in the region of 400–800 nm belonging to visible light; this result was explained due to the strong interaction among the ZnO, Bi, and Cu and the formulation of impurity energy levels within ZnO doped with them. The band gap of these samples was calculated using Tauc's formula. As shown in Fig. 10(b), the energy band gap of undoped ZnO/cotton was calculated to be 3.23 eV. However, after the doping with Bi and Cu (3% Cu, 5% Bi, and 3% Bi–5% Cu), the value of energy band gap presents a distinct reduction, 3.01 eV, 2.93 eV and 2.84 eV respectively, which was attributed to the atoms of Bi and Cu successfully replacing Zn^{2+} into the crystal and impurity levels decreasing the energy required for the electron transition from the valence to the conduction band. The results of optical properties certified a remarkable effect of Bi and Cu doping, indicating that ZnO/cotton combined with Bi and Cu enhanced the visible light absorption and perhaps enhanced the photocatalytic activity in visible light.

3.6 Photocatalysis

The photocatalytic performance of ZnO/cotton, Cu-doped ZnO/cotton, Bi-doped ZnO/cotton and Cu–Bi co-doped ZnO/cotton

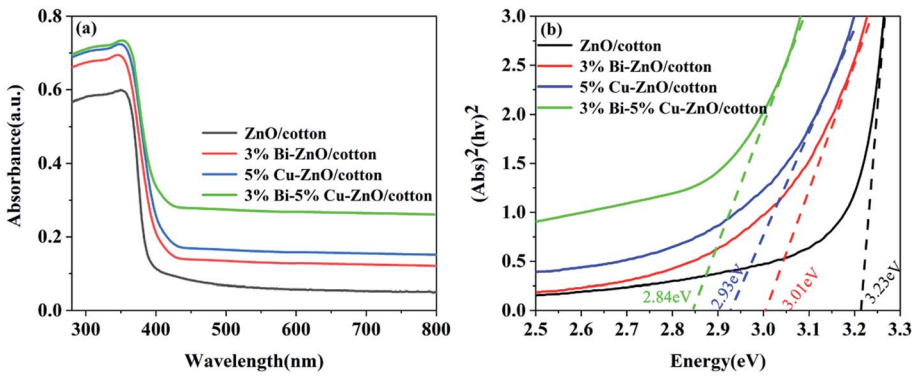

Fig. 10 UV-vis absorbance spectra of samples with different doping ratio (a) and Tauc plots (b).

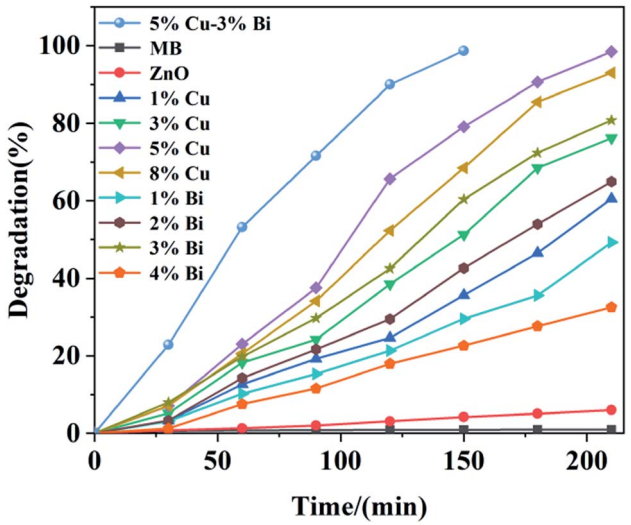

Fig. 11 The degradation rate of MB solution as a function of time with Bi, Cu doped ZnO/cotton in different proportions.

was examined *via* degradation of MB as the main dye pollutant under the visible light irradiation. As shown in Fig. 11, the degradation of MB solution only reached 6.01% after 3 h of visible irradiation with ZnO/cotton as the catalyst; this minor degradation came from the interaction between the dye and the aqueous solution and the adsorption on the surface of the cotton fabric, which was mainly attributed to the fact that ZnO is unable to respond in the visible light region so that the energy of visible light is not enough to make electrons undergo transition from the valence band to the conduction band. In contrast, 60.51%, 76.24% and 98.46% of MB dye solution degraded with 1% Cu, 3% Cu and 5% Cu doped ZnO/cotton within 3 h of visible radiation; however, when the doping amount of copper was 8%, the degradation rate was lower than that of the doping amount of 5%, because CuO appeared in the reaction system, which affects the overall catalytic effect. This result proved the successful doping of copper ions and the remarkable improvement of photocatalytic performance under visible light. Meanwhile, the degradation percentage also increased significantly as the Bi doping concentration increased (1–3%), reaching 49.25%, 64.95% and 80.79% respectively; however, the degradation rate suddenly dropped with the dosage concentration at 4% mainly due to the excessive bismuth generating a mass of divalent compound of bismuth, which reduces the photocatalytic performance; this is the fundamental reason that the photocatalytic effect of bismuth doping was not as good as copper doping.

For the 5% Cu–3% Bi co-doped sample, the degradation percentage reached 98.66% within 150 min of visible light irradiation; this degradation time was clearly shortest among all samples. Bi and Cu doping led to a significant increase in photocatalytic effect mainly due to the reduction of band gap; the valence band electron bonding energies of ZnO and 3% Bi–5% Cu/ZnO were 2.64 eV and 2.41 eV by analysing the XPS valence band spectra of the two samples in Fig. 12(a), and at the same time, the binding energies of the conduction band electrons of the two samples are −0.59 eV and −0.43 eV respectively, based on the energy difference of DRS. Fig. 12(b) is the band structure of ZnO and Bi–Cu/ZnO determined by test and calculation; it can be seen that, with the Bi and Cu doping, the band gap width of ZnO was significantly shortened, and valence band electrons were more likely to undergo electron transition, which was the main reason for the great improvement of photocatalytic performance. Related reactions in Fig. 12(b) were as follows (eqn (3)–(6)):

$$\text{Photocatalyst} \xrightarrow{h\nu} e^- + h^+ \quad (3)$$

$$H_2O + h^+ \rightarrow {}^{\cdot}OH + H^+ \quad (4)$$

$$O_2 + e^- \rightarrow {}^{\cdot}O_2 \quad (5)$$

$$\text{dyes (MB)} + {}^{\cdot}OH \rightarrow CO_2 + H_2O \quad (6)$$

$$\text{dyes (MB)} + {}^{\cdot}O_2 \rightarrow CO_2 + H_2O \quad (7)$$

4. Conclusions

In summary, Bi–Cu co-doped ZnO nanospheres were successfully grown on the surface of cotton fabric *via* a sol–gel assisted hydrothermal method, which were obtained using citric acid as a morphology control agent. SEM and XRD results demonstrate

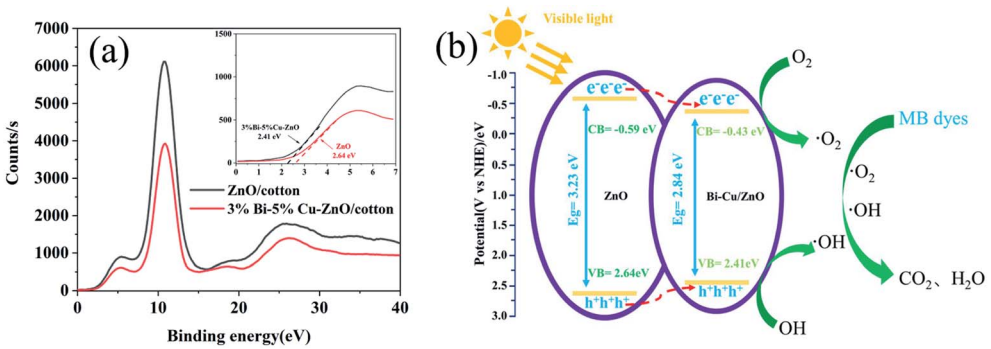

Fig. 12 XPS valence band spectra and band structures of ZnO and 3% Bi–5% Cu/ZnO.

that the ZnO nanospheres existed in the structure of hexagonal wurtzite and the doping with Bi and Cu didn't change their spherical morphology. Besides, the optimal doping ratio, 3% Bi and 5% Cu, endowed cotton fabric with excellent photocatalytic performance; the degradation of MB solution reached 98.66% under visible light irradiation for 150 min, which was mainly attributed to the ZnO energy gap decreasing from 3.23 eV to 2.84 eV through the RDS results. Meanwhile, the UPF value of the cotton fabric with 3% Bi–5% Cu doped ZnO was 375.43, and it was still 283.54 after 40 washes, which proved the outstanding UV resistance of fabric and reliable binding fastness to ZnO. In this paper, a controllable method of growing spherical nano ZnO on the surface of cotton fabric was proposed by studying the reaction factors, and Cu and Bi co-doping was adopted to give cotton fabric excellent UV resistance and photocatalytic properties, which provides a feasible scheme for controlling the morphology of nanomaterials and has a great application prospect in the future.

Conflicts of interest

All authors certify that there is no conflict of interests in this study.

Acknowledgements

The authors appreciate the laboratory and equipment provided by Shanghai University of Engineering Science and XPS, XRD analysis were provided by Shiyanjia Lab (www.shiyanjia.com).

References

1 D. Lee, D. Park, K. Shin, H. M. Seo, H. Lee, Y. Choi and J. W. Kim, ZnO nanoparticles-laden cellulose nanofibers-armored Pickering emulsions with improved UV protection and water resistance, *J. Ind. Eng. Chem.*, 2021, **96**, 219–225.

2 J. Zhang and C. Teng, Nondestructive growing nano-ZnO on aramid fibers to improve UV resistance and enhance interfacial strength in composites, *Mater. Des.*, 2020, **192**, 108774.

3 J. Yoon and S.-G. Oh, Synthesis of amine modified ZnO nanoparticles and their photocatalytic activities in micellar solutions under UV irradiation, *J. Ind. Eng. Chem.*, 2021, **96**, 390–396.

4 Z. Ren, X. Li, L. Guo, J. Wu, Y. Li, W. Liu, P. Li, Y. Fu and J. Ma, Facile synthesis of ZnO/ZnS heterojunction nanoarrays for enhanced piezo-photocatalytic performance, *Mater. Lett.*, 2021, **292**, DOI: 10.1016/J.MATLET.2021.129635.

5 Z. Gončuková, M. Řezanka, J. Dolina and L. Dvořák, Sulfonated polyethersulfone membrane doped with ZnO-APTES nanoparticles with antimicrobial properties, *React. Funct. Polym.*, 2021, **162**, DOI: 10.1016/j.reactfunctpolym.2021.104872.

6 Y. Chen, L. Xu, X. Wu and B. Xu, The influence of nano ZnO coated by phosphazene/triazine bi-group molecular on the flame retardant property and mechanical property of intumescent flame retardant poly (lactic acid) composites, *Thermochim. Acta*, 2019, **679**, 178336–178337.

7 T. Merve, D. Aslı and G. Yavuz, The synthesis and application of chitosan coated ZnO nanorods for multifunctional cotton fabrics, *Mater. Chem. Phys.*, 2021, **268**(1), 124736.

8 C. Ling and L. Guo, An eco-friendly and durable multifunctional cotton fabric incorporating ZnO and a branched polymer, *Cellulose*, 2021, **28**(9), 5843–5854.

9 M. I. H. Mondal, J. Saha and Antimicrobial, UV Resistant and Thermal Comfort Properties of Chitosan- and Aloe vera-Modified Cotton Woven Fabric, *Cellulose*, 2019, **27**(2), 405–420.

10 X. Jia, J. Y. Zhang, J. Xu, Y. Chang, F. Shi, Z. Zhang and H. Zhang, Design of functional cotton fabric *via* modified carbon nanotubes, *Pigm. Resin Technol.*, 2020, **49**(1), 71–78.

11 M. M. Iqbal, M. Imran, T. Hussain, M. A. Naeem, A. A. Al-Kahtani, G. M. Shah, S. Ahmad, A. Farooq, M. Rizwan, A. Majeed, A. R. Khan and S. Ali, Effective sequestration of Congo red dye with ZnO/cotton stalks biochar nanocomposite: modeling, reusability and stability, *J. Saudi Chem. Soc.*, 2021, **25**(2), 101176.

12 E. S. Aminloo and M. Montazer, Clean Sono-synthesis of ZnO on Cotton/Nylon Fabric Using Dopamine: Photocatalytic, Hydrophilic, Antibacterial Features, *Fibers Polym.*, 2021, **22**(1), 97–108.

13 A. Javed, M. Azeem, J. Wiener, M. Thukkaram, J. Saskova and T. Mansoor, Ultrasonically Assisted *In Situ* Deposition of ZnO Nano Particles on Cotton Fabrics for Multifunctional Textiles, *Fibers Polym.*, 2021, **22**(1), 77–86.

14 M. Z. Khan, J. Militky, V. Baheti, M. Fijalkowski, J. Wiener, L. Voleský and K. Adach, Growth of ZnO nanorods on cotton fabrics *via* microwave hydrothermal method: effect of size and shape of nanorods on superhydrophobic and UV-blocking properties, *Cellulose*, 2020, **27**(17), 10519–10539.

15 I. D. Tunç, M. Erol, F. Güneş and M. Sütçü, Growth of ZnO nanowires on carbon fibers for photocatalytic degradation of methylene blue aqueous solutions: an investigation on the optimization of processing parameters through response surface methodology/central composite design, *Ceram. Int.*, 2020, **46**(6), 7459–7474.

16 S. Luo, C. Liu, Y. Wan, W. Li, C. Ma, S. Liu, H. J. Heeres, W. Zheng, K. Seshan and S. He, Self-assembly of single-crystal ZnO nanorod arrays on flexible activated carbon fibers substrates and the superior photocatalytic degradation activity, *Appl. Surf. Sci.*, 2020, **513**, DOI: 10.1016/j.apsusc.2020.145878.

17 J. Zhang and C. Teng, Nondestructive growing nano-ZnO on aramid fibers to improve UV resistance and enhance interfacial strength in composites, *Mater. Des.*, 2020, **192**, DOI: 10.1016/j.matdes.2020.108774.

18 K. Jagajjanani Rao, T. Korumilli, K. P. Akshaykumar, S. Wacławek, M. Černík, V. Vinod and T. Padil, Development of ZnO Nanoflake Type Structures Using Silk Fibres as Template for Water Pollutants Remediation, *Polymers*, 2020, **12**(5), 1151.

19 D. Gao, J. Liu, L. Lyu, Y. Li and J. Ma, Warda Baig. Construct the Multifunction of Cotton Fabric by Synergism between Nano ZnO and Ag, *Fibers Polym.*, 2020, **21**(3), 505–512.

20 B. Hou, L. Li, X. Li, Q. Li, J. Li, H. Wang, Q. Wang, Y. Gu, B.-H. Kim and J. Huang, Influence of Bi^{3+} doping on microstructure and photoelectric properties of ZnO thin film, *Chem. Phys. Lett.*, 2021, **763**, DOI: 10.1016/J.CPLETT.2020.138174.

21 D. S. Vasanthi, K. Ravichandran, P. Kavitha, S. Sriram and P. K. Praseetha, Combined effect of Cu and N on bandgap modification of ZnO film towards effective visible light responsive photocatalytic dye degradation, *Superlattices Microstruct.*, 2020, **145**, DOI: 10.1016/j.spmi.2020.106637.

22 A. Bandyopadhyay, N. Gupta, M. Nath, S. Chakraborty and S. Sutradhar, Magnetic properties of Mn doped ZnO: A Monte Carlo simulation analysis, *Vacuum*, 2021, **183**, 109786–109795.

23 R. Nithya, S. Ragupathy, D. Sakthi, V. Arun and N. Kannadasan, A study on Mn doped ZnO loaded on CSAC for the photocatalytic degradation of brilliant green dye, *Chem. Phys. Lett.*, 2020, **755**, 137769.

24 Y. N. Wang, J. Li and Q. Wang, The performance of daylight photocatalytic activity towards degradation of MB by the flower-like and approximate flower-like complexes of graphene with ZnO and Cerium doped ZnO, *Optik*, 2020, **204**, DOI: 10.1016/j.ijleo.2019.164131.

25 Z. Li, M. Xiong, X. Li, J. Li, N. Wang and S. Zhang, First principle study of electronic structure and optical properties of Mo doped ZnO with different concentrations, *Optik*, 2021, **228**(2), 166136.

26 B. Poornaprakash, U. Chalapathi, K. Subramanyam, S. V. Prabhakar Vattikuti and S.-H. Park, Wurtzite phase Co-doped ZnO nanorods: Morphological, structural, optical, magnetic, and enhanced photocatalytic characteristics, *Ceram. Int.*, 2020, **46**(3), 2931–2939.

27 K. E. Salem, A. M. Mokhtar, I. Soliman, M. Ramadan, B. S. Shaheen and N. K. Allam, Ge-doped ZnO nanorods grown on FTO for photoelectrochemical water splitting with exceptional photoconversion efficiency, *Int. J. Hydrogen Energy*, 2021, **46**(1), 209–220.

28 M. Bandeira, M. Giovanela, M. Roesch-Ely, D. M. Devine and J. da Silva, Crespo. Green synthesis of zinc oxide nanoparticles: A review of the synthesis methodology and mechanism of formation, *Sustainable Chem. Pharm.*, 2020, **15**, 100223.

29 A. Michał, ZnO as a Functional Material, a Review, *Crystals*, 2019, **9**(10), 505.

30 T. K. Pathak, H. C. Swart and R. E. Kroon, Influence of Bi doping on the structure and photoluminescence of ZnO phosphor synthesized by the combustion method, *Spectrochim. Acta, Part A*, 2018, **190**, 164–171.

31 K. V. Chandekar, M. Shkir, B. M. Al-Shehri, S. AlFaify, R. G. Halor, A. Khan, K. S. Al-Namshah and M. S. Hamdy, Visible light sensitive Cu doped ZnO: facile synthesis, characterization and high photocatalytic response, *Mater. Charact.*, 2020, **165**, DOI: 10.1016/j.matchar.2020.110387.

32 S. Singhal, J. Kaur, T. Namgyal and R. Sharma, Cu-doped ZnO nanoparticles: synthesis, structural and electrical properties, *Phys. B*, 2012, **407**(8), 1223–1226.

33 R. Swaminathan, M. A. Willard and M. E. McHenry, Experimental observations and nucleation and growth theory of polyhedral magnetic ferrite nanoparticles synthesized using an RF plasma torch, *Acta Mater.*, 2005, **54**(3), 807–816.

34 R. Zhu, Q. Zhao, J. Xu, *et al.*, *Ab initio* thermodynamic study on two-dimensional atomic nucleation on ZnO polar surfaces, *Appl. Surf. Sci.*, 2017, **412**, 417–423.

35 H. Yang, Q. Zhang, Y. Chen, Y. Huang, F. Yang and Z. Lu, Ultrasonic-microwave synthesis of ZnO/BiOBr functionalized cotton fabrics with antibacterial and photocatalytic properties, *Carbohydr. Polym.*, 2018, **201**, 162–171.

36 Y. Chen, X. Xu, X. Li and G. Zhang, Vacancy induced room temperature ferromagnetism in Cu-doped ZnO nanofibers, *Appl. Surf. Sci.*, 2020, **506**, DOI: 10.1016/j.apsusc.2019.144905.

37 I. Jellal, K. Nouneh, H. Toura, M. Boutamart, S. Briche, J. Naja, B. M. Soucase and M. E. Touhami, Enhanced photocatalytic activity of supported Cu-doped ZnO nanostructures prepared by SILAR method, *Opt. Mater.*, 2020, DOI: 10.1016/J.OPTMAT.2020.110669.

38 N. Moraes, R. Rocha, M. Silva, *et al.*, Facile preparation of Bi-doped ZnO/β-Bi_2O_3/carbon xerogel composites towards visible-light photocatalytic applications: effect of calcination temperature and bismuth content, *Ceram. Int.*, 2020, **46**(15), 23895–23909.

39 Z. Zhang, X. Chen, J. Kang, *et al.*, The active sites of Cu–ZnO catalysts for water gas shift and CO hydrogenation reactions, *Nat. Commun.*, 2021, **12**(1), DOI: 10.1038/s41467-021-24621-8.

40 C. Z. Wu, Y. H. Liang, Y. C. Yin, M. F. Cai, J. H. Nie and S. C. Shen, Characterization of Hydrolysis Process of a Silane Coupling Agent KH-570, *Key Eng. Mater.*, 2018, **4527**, 279–285.